ナノXAFS-STEM/EDS同視野解析法による燃料電池Pt/Cカソード触媒の空間不均一劣化計測

岩　澤　康　裕*

*岩澤康裕　客員フェロー

Spatially Non-uniform Degradation Observation of PEFC Pt/C Cathode Catalysts Imaged by Same-view Nano-XAFS-STEM/EDS Technique

Yasuhiro IWASAWA*

We have visualized spatially non-uniform degradation events of Pt/C cathode catalysts in polymer electrolyte fuel cells involving the formation and dissolution of positively charged Pt ions and detachment of metallic Pt nanoparticles/clusters by a same-view nano XAFS and STEM-EDS imaging technique under humid N_2 atmosphere.

Introduction

Polymer electrolyte fuel cell (PEFC) is one of clean energy-converting devices with high power density and efficiency at low temperatures,[1,2] commercialization of the stationary fuel cell power generation system was succeeded first in Japan, 2009, and recently, the TOYOTA FC vehicle “MIRAI” was launched to a market in December 2014 and the HONDA FC vehicle “CLARITY FUEL CELL” was also launched as car-rental in March 2016. Nevertheless, for widely spread commercialization of FC vehicles, large improvements in performance per Pt and particularly reliability and durability are indispensable. To solve these problems efficiently, the characterization and understanding of electrocatalysts and fundamental issues in membrane electrode assembly (MEA) for development of next-generation PEFCs are mandatory. Particularly, it is necessary to clarify the key factors and mechanisms which degrade catalytic activities of Pt/C cathode catalysts and improve their durability to conduct repeated oxygen reduction reactions (ORR) under PEFC operating conditions. These topics have extensively been studied thus far, but the origin and detailed mechanism for the ORR promotion and degradation are still unclear.[2,3]

The ORR process on MEA Pt/C cathode catalysts in potential increasing and decreasing processes has been demonstrated to be composed of 6 elementary reaction processes involving Pt valence increase/decrease, Pt-O bond formation/dissociation and Pt-Pt bond dissociation/reformation at Pt nanoparticle surfaces.[4–10] The ORR activity and degradation of PEFCs with the 6 key reaction processes are suggested to occur heterogeneously in the 3D space of the MEA Pt/C cathode catalyst layer.[11–13] This may depend on the heterogeneous property and distribution of Pt nanoparticles and carbon supports in the cathode layer and microscopically non-uniform potentials loaded at different places of the cathode layer in PEFC potential operations. Therefore, we attempted to visualize the place and origin of the dissolution and deterioration events of the Pt/C cathode catalysts inside MEA in PEFC by the same-view nano-XAFS and STEM-EDS techniques.[12,13] PEFC MEAs have been characterized by NMR, Raman, FT-IR/ATR-IR, TEM/SEM, XRD, neutron scattering, soft-X-ray XPS, DFT calculations, etc. to understand the PEFC catalysis and deactivation.[9–21] Nevertheless, It is difficult to observe the dynamic and spatial change and behavior of Pt nanoparticle surfaces in MEAs with a stacking structure by NMR, Raman, FT-IR/ATR-IR, TEM/SEM, XRD, neutron scattering, soft-X-ray XPS, etc.

X-ray absorption fine structure (XAFS) is a unique and powerful technique, which can directly observe the molecular-level structures and electronic states of the cathode catalysts in PEFC.[4,14–21] Recently, *in situ* time-resolved XAFS has been developed to elucidate the dynamic transformations of structures and electronic states of Pt/C and Pt_3Co/C cathode catalysts in PEFC MEAs and to decide elementary steps and their rate constants for the chemical events at the cathode

2017年3月6日 受理
* 豊田理化学研究所客員フェロー
電気通信大学燃料電池イノベーション研究センター長・特任教授
東京大学名誉教授，理学博士
専門分野：触媒化学，表面科学，X線分光学

surfaces.[4–10] More recently, 2D and 3D micro and nano-scale imagings of Pt/C cathode layers in PEFCs by spatially resolved XAFS have also received much attention to identify heterogeneous spatial functions with high complexity.[11–13, 20–23] We investigated spatially non-uniform degradation of Pt/C cathode catalyst layers in PEFC MEAs by means of nano XAFS imaging and same-view nano XAFS/STEM-EDS methods at a high-performance beamline BL36XU equipped with a scanning nano XAFS analysis system,[12,13,25] which we designed and constructed at SPring-8.[24] These imaging techniques provided new insights into the origin and spatial sites of dissolution and deterioration of Pt nanoparticles in PEFC MEAs.[12, 13, 25]

In this report, we briefly summarize our recent spatially-resolved XAFS results on Pt species mapping to correlate with Pt/C deterioration, cathode crack/void sizes, and Pt/ionomer ratios.[25]

Nano-focused beam XAFS mapping

Pt L_{III}-edge nano XAFS spectra were measured in a fluorescence mode using Vortex-ME IV detector at BL36XU by using a Si(111) double crystal monochromator. X-ray beam (11.39–12.17 keV) was focused to 570 nm × 540 nm and 228 nm × 225 nm via a pair of elliptically bent Kirkpatrick-Baez (KB) mirrors. In the scanning nano XAFS method, a XAFS spectrum was obtained from totally 206 maps corresponding to 206 energy points. To avoid a sample damage, a beam stay time in a pixel point was shortened as much as possible. The exposure time in the mapping was only 6–12 μs at each pixel. In the scanning nano XAFS method, we scanned an MEA sample on a holder along a line against nano-focused X-rays at a given X-ray energy, and then scanned it on the same line at a next given energy and repeated the line scan in the energy range every 0.4 eV and 2.0 eV, respectively to obtain XANES and EXAFS spectra, and these procedures were repeated in the whole micro area of the MEA Pt/C cathode layer. These measurements give 2D XRF maps in the MEA area at each X-ray energy, from which we can extract 2D fluorescence XAFS data in the mapping area.[13,25]

Nano QXAFS mapping

In the nano QXAFS method, the MEA sample was fixed at a position during the measurement of a QEXAFS spectrum, and then the sample on the holder was moved to the next point to measure a QEXAFS spectrum again. This procedure was repeated to obtain a QEXAFS mapping in the target MEA area.[13,25]

Beam damage during the XAFS measurements

During the repeated nano QXAFS measurements 4 times (totally 20 min acquisition), there were no significant changes in the nano QXANES. However, after 5th nano QXAFS measurements (totally 25 min acquisition) after the nano XRF map, the edge jump dropped because of loss of carbon (carbon degradation) as support for Pt nanoparticles. We also measured maps with large scale (50 μm × 50 μm) before and after the nano XAFS measurements and confirmed that the sample/beam position did not change. This indicates a sample damage by X-ray nano beam irradiation. Hence, we chose the acquisition time of 15 min for measuring good nano QXAFS spectra (sum of 1st – 3rd nano QXAFS spectra) to avoid sample damage by X-ray nano beam irradiation. The sample damage by the X-ray nano-beam irradiation was also examined in the scanning nano XAFS mapping at μ(11.600 keV) over the whole region. The first and second maps were same. In the scanning nano XAFS method the nano-beam stay in the same position of the MEA piece was 8 μs. Measurement time was 1.6 s/spectrum at a nano-focused area (one pixel) and as a total of 2500 pixels the total measurement time was 1.1 h. No effects of the nano-focused X-ray irradiation on the MEA sample damage during the scanning nano XAFS mapping measurements. Thus, we could reduce sample damages from the nano-focused X-ray beam irradiation to a negligible level owing to as a shortest stay as possible of the beam on the same point of a sample (6–12 μs beam stay per pixel). The acquisition time for the scanning nano XAFS measurements was.

XAFS data analysis

The scanning nano XANES and the nano QEXAFS were used to spatially image Pt valences and bonding states, respectively. In the XANES analysis the scanning nano XANES spectra were fitted by a linear combination of the arctangent and Lorenzian functions. The values at 11.600 keV in the arctangent function were used for estimation of Pt quantity because the background in all XAFS spectra was very low. After the normalization of XANES spectra, the white line peak top (WLPT) intensity and white line peak area (WLPA) were calculated from the fitted Lorenzian function, and Pt valences in the activated and degraded MEA Pt/C samples were estimated from a linear relationship between the WLPA and Pt valence. For the position calibration of nano-XAFS map and STEM image we used the orthogonal distance regression for the estimation of fitting parameters p_0, p_1 and p_2 to give a minimum residual; $A(x,y) - p_0 * B(x\text{-}p_1, y\text{-}p_2)$, where ($A(x,y)$ and $B(x,y)$ are absorbance

of nano XAFS map and contrast of the STEM image, respectively for coordinate point (x, y)). Thus, the positions were calibrated by using the calculated p_1 and p_2.[13,25] A small distortion along x axis of XAFS map from a sample inclement angle 30° was corrected to multiply 1/cos (30°) to x axis of the obtained map.

TEM/STEM-EDS observations for the same-view with nano XAFS

TEM and STEM-EDS images were measured on EM-2100F (JEOL) equipped with an energy dispersive spectrometer (EDS) at 200 kV. STEM-EDS images were observed by electron beams with 0.7 nm of spot size, which was sufficiently smaller than the nano–micro cracks/voids (larger than 100 nm). To avoid the formation of bubbles by water boiling in the specimen and the moving and aggregation of Pt nanoparticles during the TEM observations under the humid N_2 atmosphere, the TEM images were measured by regulating the sample temperature at 300.5 K by a Cryo-holder. For the STEM-EDS observation in the same area as that of the XAFS mapping (same-view nano XAFS/STEM-EDS), a sliced MEA was used in a SiN membrane cell.[13,25] The Pt/Ionomer ratios for each pixels in EDS map were calculated by comparison of the F/Pt count ratios to the averaged ratio at different places in the as-prepared MEA with a given value of Pt/Ionomr ratio. It was confirmed from the F/S ratios that no cracks/voids were artificially produced by the additional procedures such as slicing and cutting of the MEAs.[13,25]

MEA samples for nano XAFS and STEM-EDS measurements

The activated MEA sample was applied to 5000 accelerated durability test (ADT) cycles, by which the maximum power density decreased by 11% from that of the activated MEA. After the electrochemical procedures, both anode and cathode gases were replaced by N_2 and the PEFC was left until it reached an open circuit voltage (OCV) to prevent the samples from being exposed to high potentials. The MEAs after the activation or ADT load cycles were sliced to small pieces with 1 μm thickness by an ultra-microtome. The sliced MEA piece was putted on 1 μm SiN membrane (NTT Advance Technology, Corp.), and arranged in a specially designed XAFS cell.[13] These procedures were carried out in a humid N_2-filled glove bag to keep from drying out and to avoid exposing to air. For the same-view nano XAFS /STEM-EDS measurements, the MEA was sliced to a small piece with a given dimension, and the sliced MEA piece was put on a SiN membrane substrate (100 nm thickness) with 0.5 mm × 0.5 mm window and a 100 μm thick Si frame (Alliance Bio, Inc.) in a humid N_2-filled glove bag. The sliced sample on the SiN membrane was surrounded by a TEFLON tube (300 nm thickness), and covered with another SiN membrane. In nano-XAFS measurements, the SiN stacking membrane cell with a sealed MEA sample was put on a large SiN membrane with 1 μm thickness (10 mm × 10 mm membrane with a 4 mm × 4 mm window and a 1000 μm thick Si frame (NTT Advance Technology, Corp.) and arranged in our specially designed nano-XAFS cell.[13,25] All the procedures for the sample preparation and nano-XAFS/STEM-EDS measurements after the electrochemical measurements were carried out under humid N_2 atmosphere. The resultant *ex-situ* nano-XAFS spectra and TEM/STEM-EDS images for the sliced MEAs are regarded to be equivalent to *in-situ* images for the MEAs after the activation and the ADT cycles because all the procedures are conducted under the humid N_2 atmosphere without exposing air and the degradation of MEAs is irreversible in the present time scale.

Relation among the Pt valence, Pt/ionomer ratio and micro-crack size

The relation among Pt valence, Pt/ionomer ratio and micro-crack size in the degraded MEA was investigated by the same-view nano XAFS and STEM/EDS imaging method under the humid N_2 atmosphere using a new same-view stacking membrane cell. Figure 1 shows the scanning nano Pt L_{III}-edge XANES mapping before (**Figure 1** a-d) and after (Figure 1 A-E) the ADT 5000 load cycles using the X-ray nano beam size of 228 nm × 225 nm; a and A: STEM images, b and B: Pt quantity maps, c and C: the superposition of a and b and A and B, respectively, d and D: calculated Pt valence (oxidation state) maps, and E: Pt/Ionomer ratio map calculated from EDS maps for Pt and F (originated from Nafion ionomer) elements. In the activated MEA before the ADT cycles, while there were no significant cracks, in the degraded MEA after the ADT 5000 cycles many nano-cracks were formed due to carbon corrosion. The nano-crack areas were calculated as 11.9% of the flat cathode layer. The Pt valence of the Pt/C cathode layer in the activated MEA was zero (metallic) as shown in Figure 1 d. The calculated Pt valence map for the Pt/C cathode layer in the degraded MEA (Figure 1 D) revealed the localized distribution of Pt oxidized species in nano-cracks as well as the cathode catalyst boundary region close to the electrolyte layer. It is suggested that Pt nanoparticles are first oxidized from the boundary regions of cathode catalyst layer about 3 μm far from the edge and around these nano–micro cracks, and the Pt valence on average for the Pt

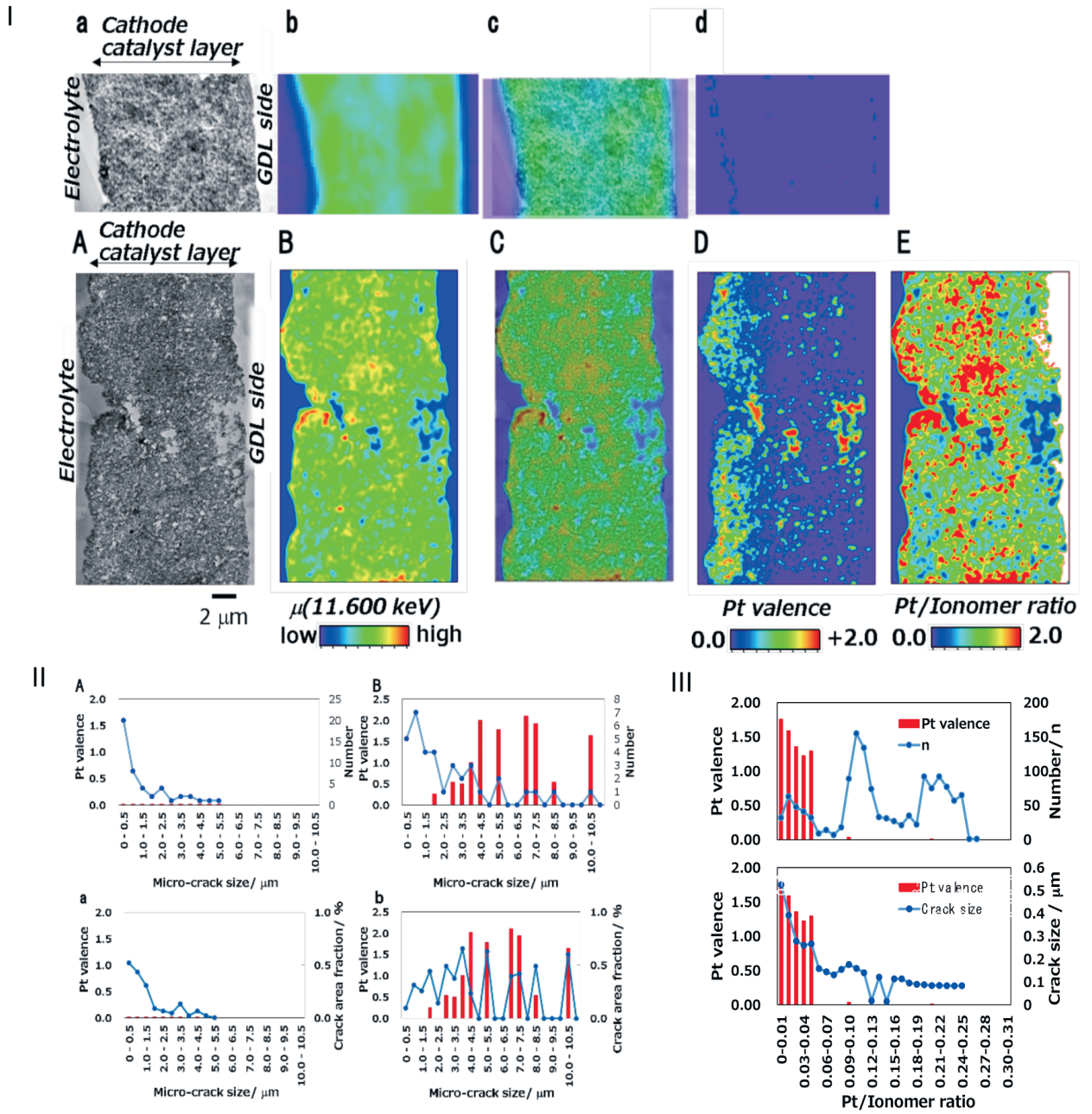

Figure 1. (Ⅰ) a, A: STEM-image, b, B: edge jump map (Pt quantity map), c, C: the superposition of a and b and A and B, respectively, and d, D: calculated Pt valence map for the MEA-B with few cracks and flat cathode catalyst surface after aging (a-d) and ADT cycles (A-D). E: Pt/Ionomer ratio map for the degraded MEA-B after the ADT cycles.
(Ⅱ) Relation between the Pt valence (red) and the number and area fraction (blue) of micro-cracks at the different sizes in the aging (A, a) and degraded (B, a) MEA-A. The data for crack size, number and area fraction, and Pt valence were taken over a wide range (ten μm scale) of the cathode layer.
(Ⅲ) The variation of the Pt/ionomer ratio with the nano-crack size and the number of for each Pt/ionomer ratio crack size, and the effect of Pt/Ionomer ratio on the Pt valence in the degraded MEA. The data for crack size, number and area fraction, and Pt valence were taken over a wide range (ten μm scale) of the cathode layer.[25]

species becomes a maximum oxidation state of 1.2+ at the edge.[25]

Figure 1 (Ⅱ) shows the plots of the Pt valences against the number and area fraction of micro-cracks at different sizes in the aging and degraded MEA, which were estimated by nano QXANES and TEM/STEM-EDS data, respectively. The sizes of micro-cracks in the activated MEA were less than 2.5 μm and the fraction of micro-crack areas in the whole cathode layer was estimated to be 1.5% by TEM/STEM-EDS data. The micro-crack sizes in the degraded MEA increased and ranged 0–5.5 μm or even more due to spatially heterogeneous carbon corrosion in the MEA Pt/C cathode layer.

The fraction of micro-crack areas increased to 3.6% after the ADT cycles (Figure 1 (Ⅱ) a and b). The Pt species in the micro-crack areas of the aging MEA-A were metallic, whereas the Pt species in the degraded MEA were oxidized, depending on the micro-crack size. The averaged Pt valence in the produced micro-cracks was estimated as 0.59+. It was found from the nano XAFS and STEM/EDS for the degraded MEA-A that the Pt species located in 2.5–4.0 μm micro-cracks possessed 0.5–1.0+ valences and the Pt species in the larger cracks than 4.0 μm showed around 2+.[25]

Figure 1 (Ⅲ) shows the variation of the Pt/ionomer ratio with the nano-crack size and the number of for each Pt/ionomer ratio crack size, and the effect of Pt/Ionomer ratio on the Pt valence in the degraded MEA. The mean crack/void size and average Pt/ionomer ratio were 154 (±130) nm and 0.14, respectively. The smaller nano-crack sizes than 200 nm were predominant in the degraded MEA after the ADT 5000 cycles, and the Pt species of ~98% among the Pt species observed in the nano-cracks existed in the nano-cracks smaller than 500 nm. The Pt valences of Pt nanoparticles in the nano-cracks larger than 250 nm were1.3–1.8+. Pt/Ionomer ratios became lower with increasing crack sizes. The tendency of easier Pt oxidation in the larger nano-cracks may be caused by an increase of electric resistance and/or heterogeneous over-loaded potentials around the nano-cracks. The content of ionomer also plays a role in the decision of Pt oxidation states for the Pt nanoparticles detached and dissoluted from the carbon suppot.[13,25] The number ratio of 80% and area ratio of 35% in the nano-cracks contained Pt and ionomers at the Pt/ionomer ratios of 0.09–0.24. The nano-cracks with the lower Pt/ionomer ratios than 0.05 included oxidized Pt species whose valences were 1.3–1.8+. On the other hand, Pt valences in the nano-cracks with the Pt/inomer ratios higher than 0.05 were calculated almost zero (metallic). These results suggest that the high content of ionomers in the nano-cracks facilitates the oxidative dissolution of Pt and stabilizes the oxidized Pt species via the coordination of Nf-SO_3 to the cationic Pt species, whereas the low content of ionomers in the nano-cracks promotes the detachment of metallic Pt nanoparticles/clusters from the carbon support into the nano-cracks.[25]

Conclusions

It was found that the catalyst degradation in the MEA with micro-cracks/holes occurred around larger cracks/holes > about 2.5 μm. The nano XAFS imaging for the MEA with few cracks/holes and a flat cathode surface could make the degraded region clearer along the depth direction. The oxidized Pt species were found in the nano-cracks/holes larger than 200 nm, and the Pt valence was nearly 2+ in the nano-cracks/holes larger than 300 nm dimension. The same-view nano-XAFS and TEM/STEM-EDS imaging provided a clear relationship between the Pt valence and Pt/ionomer ratio, which showed that the Pt valences in the nano-cracks/holes with Pt/ionomer ratio lower than 0.05 were 1.3+–1.8+. The Pt valences of Pt nanoparticles/ clusters detached from the carbon support to the nano-cracks/holes with higher Pt/ionomer ratios than 0.05 were metallic. The crack/hole size and Pt/ionomer ratio affect the degradation behavior of the Pt/C cathode catalysts in PEFC MEAs. The combination of the nano XAFS and STEM/EDS under humid N_2 atmosphere evidences the origin of the formation of Pt oxidation species and isolated Pt nanoparticles in the nano-crack/hole areas of the Pt/C cathode layer with different Pt/ionomer ratios, relevant to the degradation of PEFC catalysts. Further investigation on time-resolved chemical processes and 3D visualization at high spatial resolution is needed to evidence the detailed degradation mechanism.[25]

ACKNOWLEDGMENT

The XAFS measurements were performed with the approval of SPring-8 subject number 2010B1015, 2011A1031, 2011A1032, 2011B1039, 2011B1040, 2012A1024, 2012A1026, 2012B1024, 2013A7803, 2013B7803, 2014A7802, 2014A7806, 2014A7807, 2014B7802, 2014B7804, 2015A7804, and 2015B7804. I thanks Toyota Physical and Chemical Research Institute for supporting researches of next-generation fuel cell and green sustainable catalysis. The part of this work in collaboration with Dr. S. Takao and Iwasawa lab members was supported by the New Energy and Industrial Technology Development Organization (NEDO) of Japan.

References

1) G. Wu, K. L. More, C. M. Johnston and P. Zelenay, *Science,* **332** (2011) 443.
2) M. K. Debe, *Nature*, **486** (2012) 43.
3) C. Houchins, G. J. Kleen, J. S. Spendelow, J. Kopasz, D. Peterson, N. L. Garland, D. L. Ho, J. Marcinkoski, K. E. Martin, R. Tyler and D. C. Papageorgopoulos, *Membranes*, **2** (2012) 855.
4) M. Tada, S. Murata, T. Asakoka, K. Hiroshima, K. Okumura, H. Tanida, T. Uruga, H. Nakanishi, S. Matsumoto, Y. Inada, M. Nomura and Y. Iwasawa, *Angew. Chem. Int. Ed.*, **46** (2007) 4310.
5) N. Ishiguro, T. Saida, T. Uruga, S. Nagamatsu, O. Sekizawa, K. Nitta, T. Yamamoto, S. Ohkoshi, Y. Iwasawa, T. Yokoyama and M. Tada, *ACS Catal*., **2** (2012) 1319.
6) N. Ishiguro, T. Saida, T. Uruga, O. Sekizawa, K. Nagasawa, K. Nitta, T. Yamamoto, S. Ohkoshi, T. Yokoyama and M. Tada, *Phys. Chem. Chem. Phys.,* **15** (2013) 18827.

7) S. Nagamatsu, T. Arai, M. Yamamoto, T. Ohkura, H. Oyanagi, T. Ishizaka, H. Kawanami, T. Uruga, M. Tada and Y. Iwasawa, *J. Phys. Chem. C,* **117** (2013) 13094.
8) S. Nagamatsu, S. Takao, G. Samjeské, K. Nagasawa, O. Sekizawa, T. Kaneko, K. Higashi, T. Uruga, S. Gayen, S. Velaga, M. Sanyal and Y. Iwasawa, *Surf. Sci.,* **648** (2016) 100.
9) N. Ishiguro, S. Kityakarn, O. Sekizawa, T. Uruga, T. Sasabe, K. Nagasawa, T. Yokoyama and M. Tada, *J. Phys. Chem. C,* **118** (2014) 15874.
10) T. Kaneko, G. Samjeské, S. Nagamatsu, K. Higashi, O. Sekizawa, S. Takao, T. Yamamoto, X. Zhao, T. Sakata, T. Uruga and Y. Iwasawa, *J. Phys. Chem. C,* **120** (2016) 24250.
11) T. Saida, O. Sekizawa, N. Ishiguro, M. Hoshino, K. Uesugi, T. Uruga, S. Ohkoshi, T. Yokoyama and M. Tada, *Angew. Chem. Int. Ed.*, **124** (2012) 10457.
12) S. Takao, O. Sekizawa, S. Nagamatsu, T. Kaneko, T. Yamamoto, G. Samjeské, K. Higashi, K. Nagasawa, T. Tsuji, M. Suzuki, N. Kawamura, M. Mizumaki, T. Uruga and Y. Iwasawa, *Angew. Chem. Int. Ed.,* **53** (2014) 14110.
13) S. Takao, O. Sekizawa, G. Samjeské, S. Nagamatsu, T. Kaneko, T. Yamamoto, K. Higashi, K. Nagasawa, T. Uruga and Y. Iwasawa, *J. Phys. Chem. Lett*., **6** (2015) 2121.
14) S. Mukerjee, S. Srinivasan, M. P. Soriaga and J. McBreen, *J. Electrochem. Soc.,* **142** (1995), 1409.
15) Y. Iwasawa (Ed.) *X-ray Absorption Fine Structure for Catalysts and Surfaces*, (World Scientific Publishing: Singapore, 1996).
16) A. E. Russell and A. Rose, *Chem. Rev.,* **104** (2004) 4613.
17) R. R. Adzic, J. X. Wang, B. M. Ocko and J. McBreen, (*Handbook of Fuel Cells*: Wiley, 2010).
18) L. Liu, G. Samjeske, S. Nagamatsu, O. Sekizawa, K. Nagasawa, S. Takao, Y. Imaizumi, T. Yamamoto, T. Uruga and Y. Iwasawa, *J. Phys. Chem. C,* **116** (2012) 23453-23464.
19) K. Nagasawa, S. Takao, K. Higashi, S. Nagamatsu, G. Samjeské, Y. Imaizumi, O. Sekizawa, T. Yamamoto, T. Uruga and Y. Iwasawa, *Phys. Chem. Chem. Phys.*, **16** (2014) 10075.
20) M. Tada, T. Uruga and Y. Iwasawa, *Catal. Lett. (Silver Anniversary Special Issue),* **145** (2015) 58.
21) Y. Iwasawa, K. Asakura and M. Tada (Eds), *XAFS Techniques for Catalysts, Nanomaterials, and Surfaces*, Springer, New York (2016).
22) K. Nagasawa, S. Takao, S. Nagamatsu, G. Samjeské, O. Sekizawa, T. Kaneko, K. Higashi, T. Yamamoto, T. Uruga and Y. Iwasawa, *J. Am. Chem. Soc.*, **137** (2015) 12856.
23) N. Ishiguro, T. Uruga, O. Sekizawa, T. Tsuji, M. Suzuki, N. Kawamura, M. Mizumaki, K. Nitta, T. Yokoyama and M. Tada, *ChemPhysChem*, **15** (2014) 1563.
24) O. Sekizawa, T. Uruga, M. Tada, K. Nitta, K. Kato, H. Tanida, K. Takeshita, S. Takahashi, M. Sano, H. Aoyagi, A. Watanabe, N. Nariyama, H. Ohashi, H. Yumoto, T. Koyama, Y. Senba, T. Takeuchi, Y. Furukawa, T. Ohata, T. Matsushita, Y. Ishizawa, T. Kudo, H. Kimura, H. Yamazaki, T. Tanaka, T. Bizen, T. Seike, S. Goto, H. Ohno, M. Takata, H. Kitamura, T. Ishikawa, T. Yokoyama and Y. Iwasawa, *J. Phys. Conf. Ser.*, **430** (2013) 012020-1.
25) S. Takao, O. Sekizawa, G. Samjeské, S. Namagatsu, T. Kaneko, K. Higashi, T. Yamamoto, K. Nagasawa, X. Zhao, T. Uruga and Y. Iwasawa, *Topics Catal. (ISHHC17 issue)*, **59** (2016) 1722.